Recent progress in perovskite solar cells

M.Khalaji Assadi[a], S. Bakhoda[a,*], R. Saidur[b,c], H. Hanaei[a]

[a] Mechanical Engineering Department, Universiti Teknologi PETRONAS (UTP), Perak, Malaysia
[b] Research Centre for Nano-Materials and Energy Technology (RCNMET), School of Science and Technology, Sunway University, No. 5, Jalan Universiti, BandarSunway, 47500 Petaling Jaya, Malaysia
[c] Centre of Research Excellence in Renewable Energy (CoRE-RE), King Fahd University of Petroleum and Minerals (KFUPM), Dhahran 31261, Kingdom of Saudi Arabia

ARTICLE INFO

ABSTRACT

Perovskite hybrid solar cells are in vogue in solar cell research. Dye-sensitized solar (DSS) cells, thin film solar cell and silicon solar cell, among others, owing to their efficiencies that are comparable to crystalline Si solar cells and ease of fabrication by a low-temperature solution technique. Although perovskite solar cells have been accounted for to exhibit enhanced output of about 21% from about 9.7%, limited researches have been conducted to find out their low stability that impedes outdoor applications. The issue of degradation of perovskite and the stability of perovskite solar cells should be addressed for good reproducibility and long life time with high conversion efficiencies. The present review aims to represent an account of the advancement in the organic, inorganic perovskite solar cells and the extent of fabrication techniques with a view to understand the material efficiency relationships.

1. Introduction

Solar energy, along with wind, biomass, tidal and geothermal energy are emerging as alternate sources of energy for our energy-deprived planet. Out of the mix, solar energy is the renewable and clean type of energy that offers an answer to the increasing concern of global warming and greenhouse gases by fossil fuels. In the course of recent decades, Si solar cells have advanced tremendously both in terms of their cost of production and efficiency [1,2]. In some parts of the world, it is being delivered to the grid power at competitive costs compared to that of fossil fuels. Newer in the mix form is vapor deposited from semiconductor and thin film-based technologies like copper-indium-gallium-selenide (CIGS), CdTe [3,4], organic/inorganic solar cells, inorganic semiconductors or hybrid composites [5–10], whereby they imply as second and third generations solar cells and are pushing the borders further regarding the ease of processing, efficiency, cost and stability owing to sustained research effort in the course of the recent decade. This has resulted in the availability of commercial products from this line of solar cells to select consumers in power electronics and low power applications in buildings. For larger markets, the cost per watt has to be substantially lowered to be comparable to that of electricity generated from fossil fuels. A quantum increase in efficiency and reduction in cost for energy technologies are warranted. Recent advances in the assembling of standard silicon solar cell have guaranteed incorporation of photovoltaic in the mainstream energy mix, with

a recent forecast anticipating a third of the global electricity demand being met by photovoltaics by 2030 [1]. Silicon-based solar cell technologies offering a combination of properties such as the ease of surface passivation, low cost, hardness and high-temperature stability have made them favored options in photovoltaic applications. Technologies promising a combination of lower cost and ease of fabrication with a better energy payback matrix offer exciting opportunities to replace silicon. As a new entrant in this field, organometallic halide perovskites offer captivation prospects [11–14]. Solution process ability, broad-spectrum solar absorption, low nonradioactive recombination losses and the potential to capitalize of research and development in the field of dye-sensitized and organic solar cells provide all the right ingredients for this technology to thrive as an alternative to the dominance of silicon. The advent of hybrid perovskite has amazed the research groups in the photovoltaic field as it has demonstrated a high performance and fast growth within the last 5 years [11,15–17]. This material has caused a rise in the Power Conversion Efficiency (PCE) for photovoltaic (PV) devices up to 20% [18–21]. The name perovskites was derived from Lev A. Perovski who was a Russian mineralogist. These materials are well known for several years; however, Miyasaka et al. (2009), mentioned the early usage of solar cells [2]. They were created on dye-sensitized solar cell architecture together with a thin layer of perovskite on the mesoporous TiO_2 as an electron collector and produced 3.8% PCE. Furthermore, as a liquid corrosive electrolyte was utilized, the cell reached a stability for

---

* Corresponding author.

Nomenclature

(PSC)	Perovskite solar cell
(PCE)	Power conversion efficiency
(DSSC)	Dye-sensitized solar cell
(HTM)	Hole transport material
(ETM)	Electron transporting materials
(PTA)	Poly triarylamine
(PTAA)	poly (bis (4-phenyl) (2,4,6-trimethylphenyl) amine)
(CB)	Conduction band
(EQE)	External quantum efficiency spectra
(VASP)	Vapor- assisted solution process
(PIA)	Photoinduced absorption spectroscopy
(ssDSC)	Solid-state dye-sensitized solar cell
(P3HT)	Poly-3-hexyl thiophene
(PDPPDBTE)	(poly [2, 5-bis (2-octyldodecyl) pyrrolo [3, 4-c] pyrrole-1, 4 (2H,5H) -dione- (E)−1, 2-di (2, 2'-bithiophen-5-yl) ethene])
(LBSO)	Lanthanum (La)−doped BaSnO3

merely few minutes. Later, Park et al. obtained 6.5% PCE using the same dye-sensitized concept in 2011 [22].

In order to avoid corrosive liquid electrolyte in perovskite DSSC, [23] the solid-state electrolyte, spiroMeOTAD (2,2′,7,7′-tetrakis(N,N-di-pmethoxyphenylamine)– 9,9′-spirobifluorene) was developed to act as a hole transport material (HTM). They developed the one-step solution processable perovskite solar cells using solid-state electrolyte and successively achieved PCE of 9.7% with admirable stability, as it shown in Fig. 1 [23].

They demonstrated a high efficiency due to charge separation by the hole transfer from excited (CH_3NH_3) PbI_3 nanoparticles to the mesoscopic TiO_2 film and spiroOMeTAD, which was confirmed by femtosecond laser studies. Moreover, they highlighted that the solid hole conductor as a HTM in PSC managed to considerably improve the PCE and stability compared to liquid electrolyte-based PSC. A major advancement was made in 2012 when Snaith and Lee realized that perovskites are stable if they make contact with a solid-state hole transporter that do not need the mesoporous TiO_2 layer to transport electrons (refer to Fig. 2) [22]. They observed high efficiency (~10%) when compared to previous dye-sensitized solar cells (DSSC) where liquid electrolyte was used.

Meanwhile, Heo et al. [24] achieved a PCE of 12% by using both flexible layers consisting of perovskite layer overlying the scaffolding TiO_2 infiltrated by perovskite. They studied several HTMs-based PSC including spiroOMeTAD and polytriarylamine and found that poly triarylamine (PTA)-based PSC achieved the highest efficiency compared to others. Later, Seok and co-workers further improved PCE to 12.3% using mixed-halide $CH_3NH_3PbI_3$–xBr_x perovskites [25]. Subsequent addition of low ionic radius of Br (10–20%) to the mixed halides allowed significant improvement in efficiency and stability due to the tetragonal to pseudo-cubic structural transition of perovskites. [26] Another researcher, Zhang (2015) developed pinhole-free perovskite films and achieved PCE of 15.2% using non-halide ($PbAc_2$) under one sun illumination. They prepared films using one-step coating method followed by annealing. Likewise, devices were also fabricated with $PbCl_2$ and PbI_2 and significant improvement in efficiency was observed. Burschka et al. showed that a technique of deposition for the sensitized architecture exceeds the efficiency of 15% by a 2-step solution process [27], while Liu et al. observed that planar solar cells can be made by thermal evaporation and have an efficiency of more than 15% [28–30].

These results suggest that deposition approaches significantly influence PCE of PSC and achieved the highest efficiency when compared to solution-processed solar cells. Later, Jeon et al. achieved PCE of 16.2% by altering the energy levels of mixed-halide $CH_3NH_3PbI_{3-x}Br_x$ with PTAA (HTM) [31]. The efficiency was further improved to 17.9% by adjusting the ratio of thickness for perovskite infiltrated TiO_2 scaffolding linked to the constant perovskite layer. Recently, Zhou et al. [32] have developed perovskite devices and achieved the highest PCE of 19.3% by adjusting the band alignment of HTM/ETM to the perovskite layer. In 2015, researchers from KRICT attained an alternate efficiency around 20.1% [33]. Shin et al. [34], studied the superoxide colloidal solution route for preparing an LBSO electrode under very mild conditions (below 300 °C). The PSCs that were fabricated with LBSO and methylammonium lead iodide ($MAPbI_3$) show a steady-state power conversion efficiency of 21.2% versus 19.7% for an mp-TiO_2 device. The LBSO-based PSCs could retain 93% of its initial performance after 1000 h of full sun illumination.

The objective of this paper is to study the structure, fabrication and mechanisms of Perovskite Solar Cells. It gives no doubt that to deal with high-efficiency and stable devices, as well as environmentally benign perovskites are the critical, yet challenging aspects of PSC research. This research has investigated the photovoltaic systems with organometal halide perovskite compounds and propose avenues for further development. The rest of this paper is organized as follows: Section 2 provides the structure of organolead halide perovskite. The optical and electrical characteristics of these halides are reviewed and
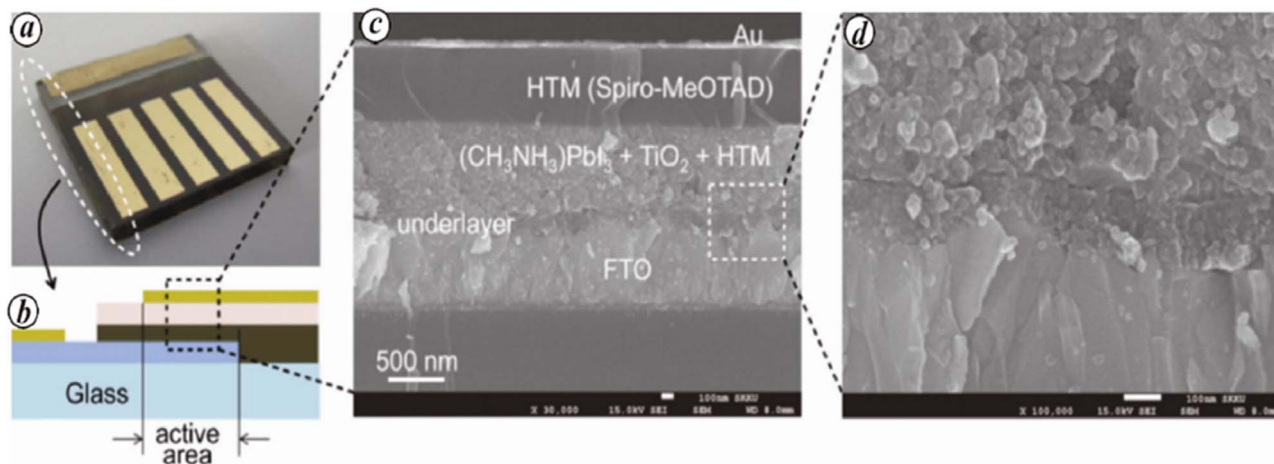

Fig. 1. a, b, Real solid state and schematic representation of the perovskite device. c, d, SEM image of the device and high-resolution image of perovskite layer [23].
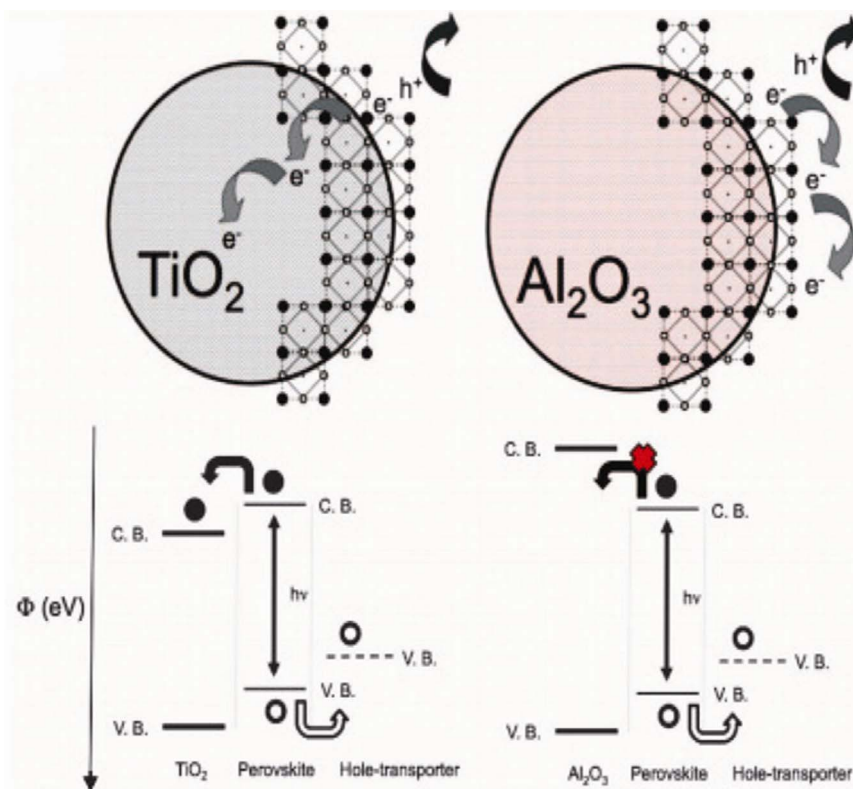
Fig. 2. Schematic representation of charge transport and transfer in perovskite-sensitized TiO₂ and Al₂O₃-based solar cells and corresponding energy levels [22].

compared to other sensitizers in Section 3. The wide variety of device architectures employed so far, are evaluated in Sections 4, 5 and 6. Since different architectures have diverse principles determining their performance, these insights into the working mechanisms allow the determination of the optimum approach. At the end, in Sections 7 and 8, future perspectives with a particular focus in the improvement of efficiency, stability of perovskites along with conclusions are discussed.

2. Structure of organolead halide perovskite

Among the various structure of perovskite, the general formula of ABX₃, the cation of A is occupied in a cube-octahedral site and the cation of B is occupied in an octahedral site (Fig. 3a) where (X = oxygen, carbon, nitrogen or halogen). Hence, A is divalent and B is tetravalent when O_2^- anion is used. Though, perovskite holding halogen anions let divalent B and monovalent A cations in sites to achieve neutrality charge. As shown in Fig. 3b, A-site cation is $CH_3NH_3^+$ and the B-site cation is Pb^{2+} in $CH_3NH_3PbI_3$.

Methylammonium lead iodide (MAPbI₃) shows considerable optical and electronic characteristics [30,35] when the band gap is 1.55 eV compared to an absorption start from 800 nm and is a decent absorber over the whole visible spectral region [35,36]. A weak binding of under 50 meV [37,38] in the photon-created excitons are separated quickly into free cations at room temperature [39]. Electrons and holes; therefore, generated a display of little efficient masses bringing about high transporter nobilities of 27 ± 7 cm² V⁻¹ S⁻¹ for electrons and 105 ± 35 cm² V⁻¹ S⁻¹ for holes [40]. Therefore, on a period size of several nanoseconds, their recombination happens and brings about non-bearer diffusion length that is the normal separation that can be secured by the transporter before the recombination, extending some-where around 100 nm and 1000 nm [40–42]. Currently, there are insufficient writings on the half and half perovskites in photovoltaic applications [43,44]. Iodine in perovskites has been substituted by different halogen yet their part is still under investigation: Cl⁻ and Br⁻

permit nonstop tuning of optical band gap and cover the vast majority of the visible spectral region [Fig. 4, a-c] [45–48]. Br- raises the conduction band and brings down the valance band where 2.2 eV is the band gap. Unfortunately, the large band gap of $CH_3NH_3PbBr_3$ restrict the light absorption with wavelength below 550 nm that cut down the photocurrent greatly. Photon-generated excitons of CH3NH3PbBr3 have 150 meV energy of binding that is greater than $CH_3NH_3PbI_3$ which is around 50 meV [36,44]. Thus, the PCE of PSCs applying $CH_3NH_3PbBr_3$ is less than $CH_3NH_3PbI_3$ [47]. In this light, the amount of 1060 nm incident photon threshold was extended to the current devices efficiency (Fig. 4 (d) and (e)).

The perovskite arrangement is approximated on its geometric tolerance factor (t) [15],

$$t = (rA + rX)/[(rB + rX)]^{1/2} \qquad (1)$$

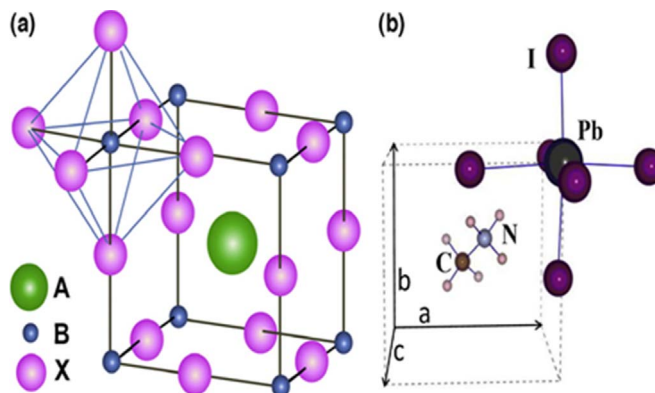where rA, rB and rX are the efficient ionic radii for A, B and X particles,

Fig. 3. (a) ABX₃ perovskite structure showing BX6 octahedral and larger A cation occupied in cubo-octahedral site. (b) Unit cell of cubic CH₃NH₃PbI₃ perovskite. [49].

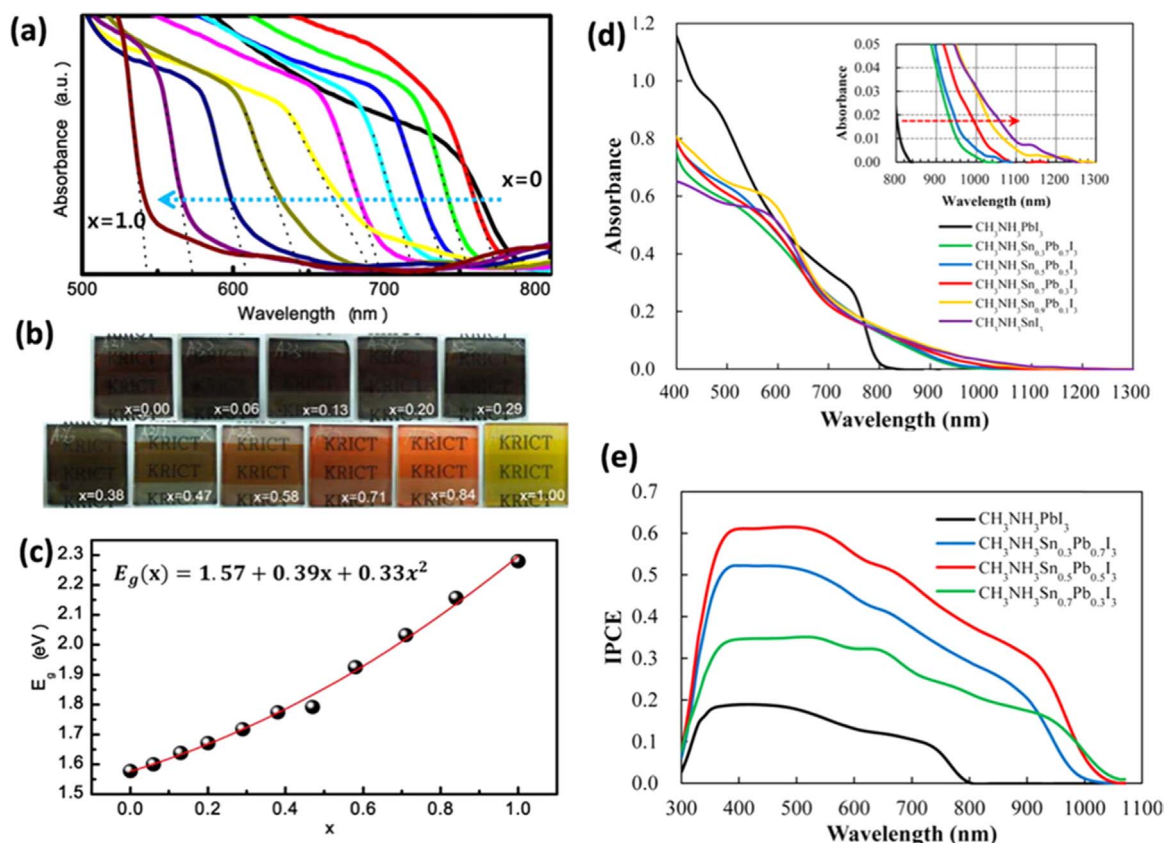**Fig. 4.** The MAPb $(I_{1-x}Br_x)_3$ UV–vis absorption spectra and the photographs Absorption evaluated for various TiO_2/CH_3NH_3Pb $(I_{1-x} Br_x)_3$ films. (b) Image of 3-D TiO_2/MAPb $(I_{1-x}Br_x)_3$ FTO glass substrates coated with double layer Nanocomposites. (c) Band gaps of $MAPb(I_{1-x}Br_x)_3$ quadratic relationship for a Br composition function (x) [25].(d) Electronic absorption spectra of porous TiO_2 on $MASn_xPb_{(1-x)}I_3$ perovskite solar cell (e) efficiency curves for incident photon-to-current conversion [50].

individually. For the transition of metal cations that are contain perovskite oxide, a perfect cubic perovskite is anticipated when t = 1. However, octahedral distortion is assessed when t < 1 [16]. Symmetry is diminished for t < 1, which influences electronic characteristics [16]. For alkali metal halide perovskite, formability is anticipated for 0.813 < t < 1.107 [17]. As it stated in Table 1, the rA in $APbX_3$ (X = Cl, Br, I) perovskite was computed for t = 0.8 and t = 1 taking into account efficient ionic radii [11]. As the tolerance of $CH_3NH_3PbI_3$ was measured as 0.83, in this manner, the deviation from a perfect cubic structure is likely to happen.

2.1. Crystal structures

Tentatively, some former investigations that are accounted for ABX_3 show different phases under various temperatures yet in the high-temperature phase, the results demonstrate similar cubic perovskite structure, as appeared in Fig. 3, where a three-dimensional structure of corner sharing BX_6 octahedron is given [7,8,19,22,32,51–55]. As a simple approach, we would only look at the cubic structure in this work to realize the chemical orientation of this sort of materials. First, we should relax the structures of all the cubic ABX_3 type compounds. The lattice constants are consolidated in Table 2. By increasing the size of X from Cl to I, we managed to get the lattice constants of ABX_3 to also increase. By keeping the B site and X site atoms, the lattice constants of ABX_3 will change with the size of A site atom. CH_3NH_3 and NH_2CHNH_2 have similar size and larger than Cs, so the lattice constants are almost the same for A=CH_3NH_3 and NH_2CHNH_2 and they are larger than that with Cs. In the event that we contrasted the acquired lattice constants and the accessible exploratory results, we can see that our outcomes are in great concurrence with the experimental data [7,8,19,32,51–53].

3. Organolead halide perovskites properties

The rapid grow of perovskite solar cells caused the achievement of near 21% of efficiency in few years. The importance of perovskite solar cells leads them to involve in many of application due to their high performance. There are three essential properties which privilege them comparing with other semiconductors and dyes types employed for light harvesting in solar cells as follow;

3.1. Organic/inorganic metal halides as light absorbers

The first advantage of the organolead halide perovskites compare with dyes is that they have a greater absorbance in the range over the entire visible to near infrared (NI). The molar extinction coefficient (MEC) of $CH_3NH_3PbI_3$ for example, is around 1.5×10^5 (mol/ L)$^{-1}$ cm^{-1} at 550 nm that is almost three times greater than organic dyes MEC achieved in solid-state DSSCs [56]. This advantage allows the perovskite absorb complete light in films when the thickness range is 500–600 nm to stunned the limitations of thickness (around 2 μm) of the usual solid_state DSSCs.

The Organic perovskites similar to the inorganic perovskites are

Table 1

A cation radii estimation in $APbX_3$ (an Effective ionic radii for coordination number of 6, b rA = t. [(rB + rX)] 1/2 - rX.).

r_{Pb} [a]	X [a]	r_A [b] for t=0.8	r_A[b] (Å) for t=1.0
Pb^{2+}(1.19 Å)	Cl$^-$ (r_{Cl} = 1.81 Å)	1.58 Å	2.43 Å
	Br$^-$ (r_{Br} = 1.96 Å)	1.60 Å	2.50 Å
	I$^-$ (r_I = 2.20 Å)	1.64 Å	2.59 Å

Table 2
Calculated lattice constants (in Å) of ABX_3 compounds (with A=Cs, CH_3NH_3, NH_2CHNH_2; B= Sn,Pb;X= Cl,Br,I). The available experimental results are shown in parentheses.

A=Cs		X		
		Cl	Br	I
B	Sn	5.61(5.60[18])	50.89	6.28(6.22[19])
	Pb	5.73(5.61[21])	5.99	6.39
A = CH₃NH₃		**X**		
		Cl	Br	I
B	Sn	5.90(5.76[18])	6.10(5.8[98])	6.41(6.2[47])
	Pb	5.80(5.68[20])	6.10(5.90[20])	6.46(6.33[20])
A=NH₂CHNH₂		**X**		
		Cl	Br	I
B	Sn	5.92	6.13	6.46(6.32[22])
	Pb	5.81	6.09	6.47

hybrid layered materials usually with an ABX_3 structure where A consider as a large cation when B is the smaller metal cation and X represent an anion from the halide series. They are able to form as an octahedral structure of BX_6, which forms a 3-D structure linked from the corners [57–59] as illustrated in Fig. 3a. The component A fills the coordinated space between the octahedrals which shape in these 3-D structures. One of the influential factor pf the cation A is its size that assists the formation of a closed packed perovskite structure as this cation is required to fit appropriately into the space composed of the four octahedra that are attached each other via their shared corners [60]. It should be consider that the organic cations are small and are limited to ethylammonium, methylammonium and formamidinium typically. The integration of larger molecules with terminal cationic groups within the inorganic framework has also been demonstrated in some cases [61,62]. The metal cations for instance, Pb^{2+}, Sn^{2+} and Ge^{2+} are usually divalent metal ions while the halide anions are I, Cl and Br. The optical absorption as well as photoluminescence is related to the metal halide employed, with the iodides resulting in smaller bandgaps and light emission at longer wavelengths while the bromides display higher bandgap and luminescence at shorter wavelengths [63–65]. Interestingly, a perovskite structure which integrates two halides (iodide and bromide) allows for the continuous alteration of the bandgap (Fig. 4a and b) [25,44]. The best solar cells have been obtained from $CH_3NH_3PbI_3$ which has a bandgap of 1.55 eV, near the optimal one for photovoltaic performance (1.4 eV). This coupled with the high extinction coefficient (greater than standard dyes [43]) enables excellent external quantum efficiency spectra (EQE) in the solar cells [23,56] until 800 nm, to harvest the photons in the visible range of the solar spectra and part of the NI (see Fig. 5). Remarkably, when $CH_3NH_3PbI_3$ is heated above 55–60⁰C, it undergoes a phase transition from tetragonal form to cubic formation [59], which is expected to narrow the bandgap.

3.2. Ambipolar organolead halide perovskites

Research on mesoporous $TiO_2/CH_3NH_3PbI_3$ solar cell [53] with about 5.5% efficiency indicated that organolead halide perovskites exhibit p-type. On the other hand, n-type behavior [66] of $CH_3NH_3PbI_3$ in non-sensitized cells of mesoporous $ZnO_2/CH_3NH_3PbI_3/spiroMeOTDA$ configuration, exhibited 10.8% efficiency [66]. This proves that $CH_3NH_3PbI_3$ exhibits ambipolar charge transfer characteristics. Additionally, n-type charge transport was demonstrated in mesoscopic Al_2O_3/mixed with halide $CH_3NH_3PbI_{3-x}Cl_x$ device [22] and the planar heterojunction perovskites exhibit ambipolar transport characteristics and are potentially excellent materials for solar cells to ensure higher photovoltaic performances. Hence, $CH_3NH_3PbI_3$ must reveal ambipolar charge transport characteristics. In Snaith's mesoscopic Al_2O_3/mixed halide $CH_3NH_3PbI_{3-x}Cl_x$ device [22] and the planar

heterojunction perovskite cells in the range of 10–15.4% efficiencies [51] were illustrated to carry the n-type charge transport. Thus, the organolead halide perovskites can show ambipolar charge transport. This state that are potential material to be applied in solar cells with numerous types of configurations to obtain the higher photovoltaic performance.

3.3. Charge transport characteristics of organolead halide perovskites

Organolead halide perovskite displays improved charge transport qualities contrasted with organic solar cells because of Wannier_type excitons in the previous and Frenkel excitons in the last mention. The transient absorption spectroscopy has been utilized to investigate the dispersion lengths of the electrons and holes in $CH_3NH_3PbI_3$ and $CH_3NH_3PbI_{3-x}Cl_x$ and observed to be 130 nm and 100 nm in $CH_3NH_3PbI_3$ and 1100 nm and 1200 nm, separately, in $CH_3NH_3PbI_{3-x}Cl_x$ [41,42]. It is realized that mesoscopic sensitized devices are favored if the dispersion length of the charge bearers is less than the profundity of higher absorption. It can be an explanation behind improved charge transport in perovskites and is a basic configuration parameter. For example, 500–600 nm is the absorption depth of organolead halide perovskites so the mesoscopic sensitized devices are favored if the depth of the light absorption is higher than the length of diffusion for the charge carriers.

It is seen in $CH_3NH_3PbI_3$ as a light absorber and shows an effectiveness of 15% [19]. Organolead halide perovskite solar cells display high transporter mobilities, quicker charge generation and adjusted charge bearer mobilities. Manufacture of devices is moderately simple from their solution and being exceptionally crystalline is generally flaw-free [39]. Therefore, due to those qualities, the examination of perovskite solar cells is less complex compared to other photovoltaic structures.

4. Fabrication of MAPBI₃

Fabrication of MAPBI₃ pervoskite is followed by two methods: one is by spin coating a solution of CH_3NH_3 and PBI_2 or spin coating PBI_2 will be continued by deposition of CH_3NH_3 that is a two-step method (Fig. 6a and b). The one-step coating method almost is the most preferred process. The way of the dissolvable (DMF, GBL or DMSO) and the difficulties in getting pin hole free perovskite highly influence the device's performance [22,36,67]. Controlling crystallinity, dewetting and related issues of roughening in pervskite films influence the implementation adversely [68].

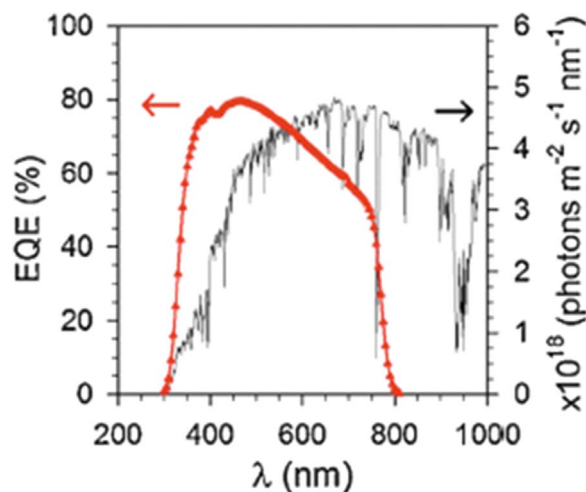In spite of these difficulties, device efficiencies of 12%, 11.8%, and

Fig. 5. The efficiency of external quantum measured for a $CH_3NH_3PbI_3$ perovskite solar cell and AM1.5 g solar spectra.
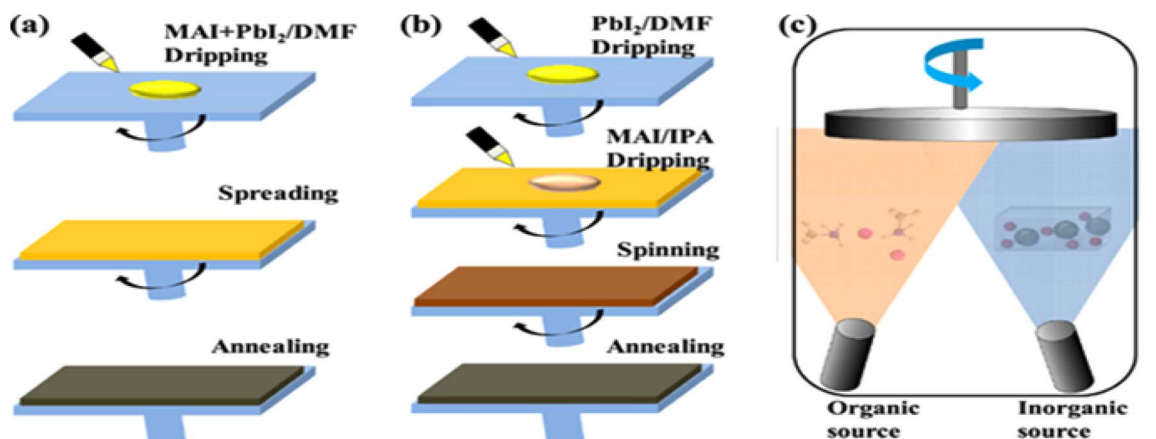
Fig. 6. perovskite active layers preparing techniques.
(a) precursor deposition in One-step, (b) sequential deposition technique in two-step, (c) vapor deposition in dual-source [69].

9.93%, separately, were obtained when CH$_3$NH$_3$Cl [70], 1, 8-diiodooctane [71] or NH$_4$Cl [72] were purposely spiked to the solution in fabrication.

5. Vapor-assisted film deposition method

Despite the ease of fabrication of the device from a solution, vapor deposition technique offers a very superior device and superior performance. The films that were obtained are uniform and the crystalline platelets are on the nanometer scale; pin hole free perovskite films are known to yield an efficiency of 15.4% [51]. Snaith et al. demonstrated a dual-source evaporation technique where CH$_3$NH$_3$I and PbCl$_2$ are pre-heated to 120 °C and 325 °C, respectively and simultaneously deposited on a TiO$_2$ coated fluorine doped tin oxide glass under high vacuum. The method is very effective high temperature and high vacuum conditions notwithstanding. Alternate methods research in the literature is deposition of a perovskite layer low temperature by "vapor- assisted solution process"(VASP) as it shown in Fig. 7. Here, the perovskite film is grown via in situ reaction of the as-deposited PBI$_2$ and CH$_3$NH$_3$I vapor [69]. These methods offer a simple and scalable process and are amenable to study the perovskite layer thickness and optoelectronic properties. This method was also examined for the inverted planar perovskite device and CH$_3$NH$_3$PBI$_3$ layers of different thickness were formed and were used for light harvesting [37].

6. Solar cell device architectures

Researchers' growing interest in CH$_3$NH$_3$PbI$_3$ perovskite is attributed to the high efficiencies and the novel configurations made possible by the singular characteristic of the material. Metal halide-based devices with a structure similar to the classical ssDSC [23] were fabricated with the organic/inorganic halide being deposited in a nanostructured layer of TiO$_2$ by a single step spin-coating method (device structure in Fig. 8a. and spiroOMeTAD (2,2',7,7'-tetrakis-(N,N-di-p-methoxyphenylamine) 9, 9'-spirobifluorene) HTM deposited on top. In this research, optical measurements show charge injection from the perovskite into TiO$_2$ (electrons) and HTM (holes) but the latter is the fastest one. Recently, the application of the sequential deposition process whereby PbI2 was converted into CH$_3$NH$_3$PbI$_3$ within the pores of the TiO$_2$ resulted in record efficiencies (η = 15.0%) [74].

The above architecture has an important alteration that replaced the TiO$_2$ mesoporous by an insulating Al$_2$O$_3$ scaffold resulting to an achievement of 10.9% of efficiency [76].

PIA measurements of CH$_3$NH$_3$PbI$_{3-x}$Cl$_x$/spiroOMeTAD layers indicated that the photogenerated hole was injected into spiroOMeTAD that avoids the voltage drop related to the concentration of the TiO$_2$ band-tails [77], which results higher photovoltage. Additionally, small-perturbation transient photocurrent decay measurements [22] also show quicker charge collection in
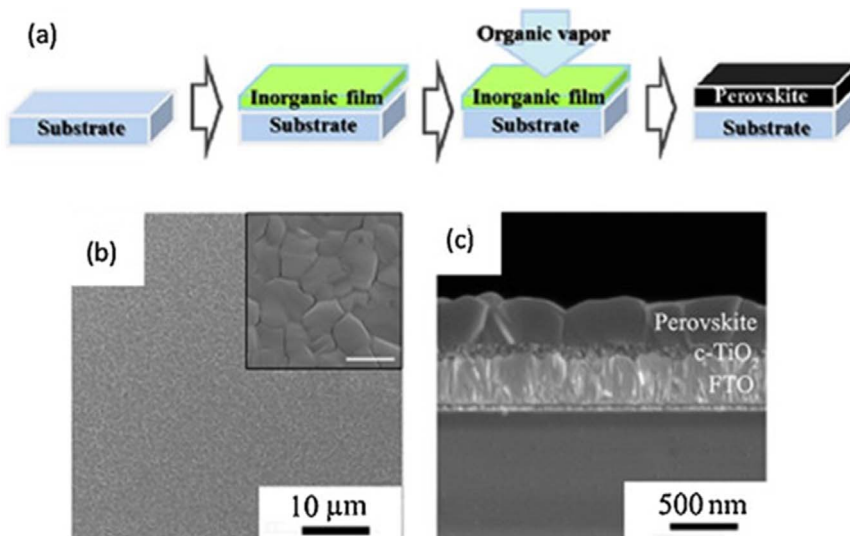

Fig. 7. (a) A schematic view (b, c) Vapor-assisted solution process using SEM imaging for deposition of perovskite film [73].
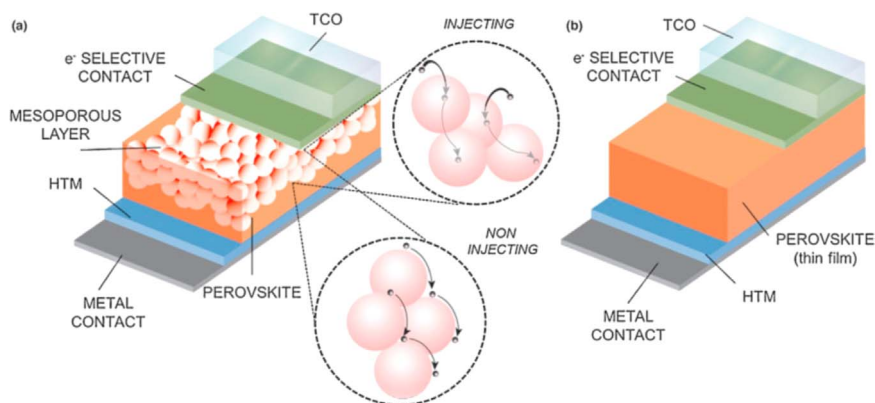
Fig. 8. The structure of (a) mesoporous perovskite solar cell with no HTM interpenetration. The electron charge transport procedure for both injecting and non-injecting mesoporous materials (b) A solar cell included thin film-like perovskite [75].

Al_2O_3 comparing with the TiO_2 (Fig. 9d). Similar results were obtained with pure $CH_3NH_3PbI_3$ in combination with non-injecting ZnO_2 scaffolds [78]. The highest photovoltage accounted so far within these class of materials (1.3 V) was also employed this configuration [79]. Interestingly, it was also announced that $CH_3NH_3PbI_3$ perovskite functions concurrently as a hole transporting material and light absorber with 5.5% conversion efficiency attained with a $TiO_2/CH_3NH_3PbI_3$ perovskite/Au construction [80]. Obviously, a good coverage of the TiO_2 film by the $CH_3NH_3PbI_3$ is needed in this case, resulting in a thin capping layer, this configuration corresponding to Fig. 8a. without the HTM layer. Also, in the absence of mesoporous films photocurrent densities close to 15 mA cm^{-2} were achieved in an approach analogous to the classical thin film architecture represented in Fig. 8b. (without scaffold) or even higher with a minimum scaffold holding the perovskite thin film (Fig. 9b).

7. Photovoltaic operational mechanisms

If we consider the system purely analogous to a solid-state dye-sensitized solar cell where the absorbed photon is converted into charge by the injection of the electrons and the regeneration of the holes, (inset Fig. 8a) certain features must be considered for understanding the main physical processes governing the cell behavior.

This model involves a fast injection of carriers from the light absorber into their respective conductive media, with no carrier transport occurring within the absorber itself. In this case, a good distribution of the absorber within the mesoporous layer will ensure maximal interfacial area required to generate the photocurrent. Thus, the limitations of this architecture will be analogous to that of the classical ssDSC [81] which have been widely studied. One of the main considerations is the light absorption. As described before, the bandgap of $CH_3NH_3PbI_3$ is near to the optimum condition for photovoltaic
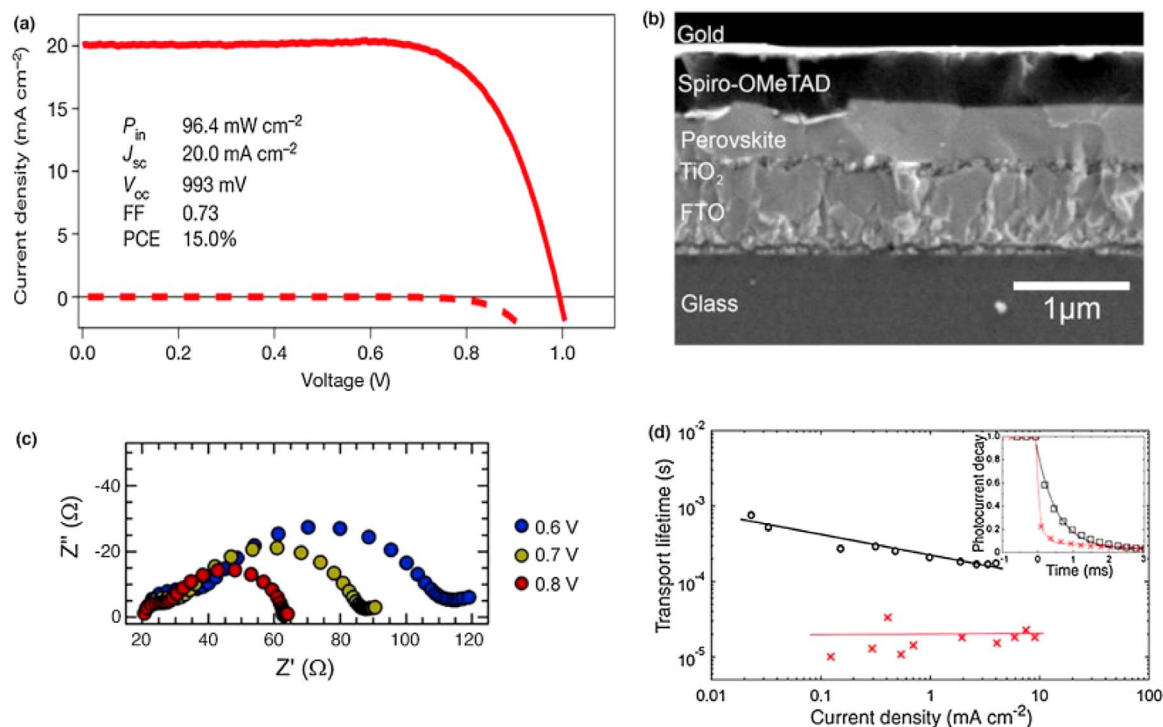

Fig. 9. (a). Measured current–voltage curve and record performance of $CH_3NH_3PbI_3$ solar cell [1], (b) cross section measured for a thin film-like perovskite solar cell with thin framework thickness [68], (c) impedance spectra measured for a nanorod/$CH_3NH_3PbI_3$solar cell [56] and (d) charge transport lifetime illustrated by the small perturbation transient photocurrent decay of perovskite sensitized TiO_2 (black line with circles to aid the eye) and Al_2O_3cells (red line with crosses). The addition shows photocurrent transients which are normalized for TiO_2 (black) and Al_2O_3 cells (red) [22].

conversion, while the high extinction coefficient of the material ensures a good absorption of the light at low mesoporous film thickness (w.r.t. dye-sensitized systems). However, for separating the excited state into charge carriers, an energy price has to be paid for both electron and hole injection-directly reflected in the achievable VOC. When TiO_2 and spiroOMeTAD are used, the energetic offsets are $\Delta E \sim 0.07$ eV and $\Delta E \sim 0.21$ eV for electrons and holes respectively (Fig. 10 and Fig. 11 a). In contrast, the energetic states distribution in the transport materials (TiO_2, HTMs) has an effect in the separation of the Fermi levels and in the charge transport due to the population of band-tails [77].

In addition to these voltage losses related to energy level mismatches similar to the charge separation, charge recombination can further limit the performance of these devices. In similar solid-state systems such as $TiO_2/Sb_2S_3/CuSCN$, the bandgap of the absorber (1.65 eV) minus the offset for electron and hole injection indicates 1.30 eV available as a potential difference; however, the reported V_{OC} at 1 sun is only 0.60 V [83]. In comparison, for $TiO_2/CH_3NH_3PbI_3/$ spiroOMeTAD devices with available potential difference is 1.22 eV while the V_{OC} achieved is more than 0.9 V [23]. This means that ~0.7 V is 'lost' in the Sb_2S_3 system, while only ~0.3 V is lost in the perovskite system. Additional experiments to compare the $CH_3NH_3PbI_3$ system against other sensitizers under similar device conditions are therefore required.

Another loss mechanism that affects the performance is manifested when varying the film's thickness [23] and [24]. Thicker films increase the light absorption but at the same time reduce the EQE and consequently the current, in contrast to classical liquid DSCs. Therefore, even after considering the encouraging open circuit potentials, the identification of the process controlling the recombination mechanism, its characterization and reduction are important for improving the efficiency of perovskites solar cells. Optical measurements such as photoinduced absorption spectroscopy (PIA) [84] and transient grating (LF-HD-TG) technique [85], electrochemical impedance spectroscopy [86] as well as mixed techniques such as transient photovoltage [87] have been used to characterize these losses with good accuracy in sensitized devices. Recently, some of these techniques have been applied to organic/inorganic halides solar cells for different absorbers and HTM [88]. Nevertheless, further investigation is needed to understand which recombination process is the dominating one in this new kind of systems.

In contrast to the sensitized solar cell architecture presented above, in solar cells utilizing mesoporous Al_2O_3 instead of mesoporous TiO_2 [89] and [22], given the energetics of alumina, the electrons injection from the absorber is not possible. Therefore, the extracted electrons must suspend within the $CH_3NH_3PbI_{3-x}Cl_x$ itself. As seen in previous sections, analogous cases are accounted where the absorber materials to transport the holes [80]. This configuration thus resembles a thin film solar cell with the scaffold providing roughness to load the

absorber layer resulting in efficient light absorption. In order to understand how this thin film configuration works, the nature of the first excited state is an important parameter for consideration. If the binding energy of the photogenerated electron–hole pair is low enough (comparable to thermal energy), charge generation can occur within the absorber. It could be beneficial for the device efficiency since the voltage drop due to the driving force needed to dissociate electron–hole pair can be avoided. Classical studies indicate that the generated electron–hole pair seems to behave as a Mott–Wannier exciton in the $CH_3NH_3PbI_3$ with low binding energies of 50 meV [63]. This indicates the possibility of the charge separation within the absorber itself. Electron and hole carrier diffusion lengths can be measured in the layers of perovskite by combining them through selective electron or hole acceptors in a bilayer configuration. Primary measurements on such bilayers have shown that electron and hole transport lengths in the perovskite films are balanced and at least 100 nm [90]. These results justify the best performance obtained in almost thick layers (~350 nm) of $CH_3NH_3PbI_{3-x}Cl_x$[90] and [68], where the device configuration was planar. Increasing the permittivity of the material (leading to low electron–hole binding energy) can enhance the charge generation.

Basic questions are still open and it is an urgent requirement to determine the optimal configuration for these solar cells. Deeper research of this matter can open new pathways to increase the efficiency of the device by first learning on the working principle.

8. Improvement on the stability of perovskites from 2009 until present

Today's perovskite-based solar cells reached a PCE of over 21.2%; however, durability is still a significant matter to consider in practical applications. The major drawback in PSC is fairly short lifetime attained with existing processes. In order to commercialize these solar cells, economically viable device with extended lifetime will be necessary. Miyasaka et al. (2009), mentioned the primary usage of solar cells [2]. It was created on dye-sensitized solar cell design together with a thin layer of perovskite on mesoporous TiO_2 as an electron collector with the iodide (I^-/I^{-3}) ($CH_3NH_3PbI_3$) produced 3.8% PCE. The stability of PSCs was enhanced from few minutes to more than 490 h applying spiroMeOTAD as a solid-state HTM in 2012 [23]. This progress is attributed to the finding of solid hole conductor. Further improvement in the stability over 500 h was achieved by another approach for example, a long-term light soaking when the light intensity was 100 mW cm^{-2} in a temperature of 450 C. However, a cell architecture that includes organic hole-transport materials (HTMs) such as poly (bis (4-phenyl) (2,4,6-trimethylphenyl) amine) (PTAA) or spiroOMeTAD, is inappropriate for estimating the influence of n-type materials on the photostability for long-term measurements (~1000 h) because organic HTMs can degrade the PV performance
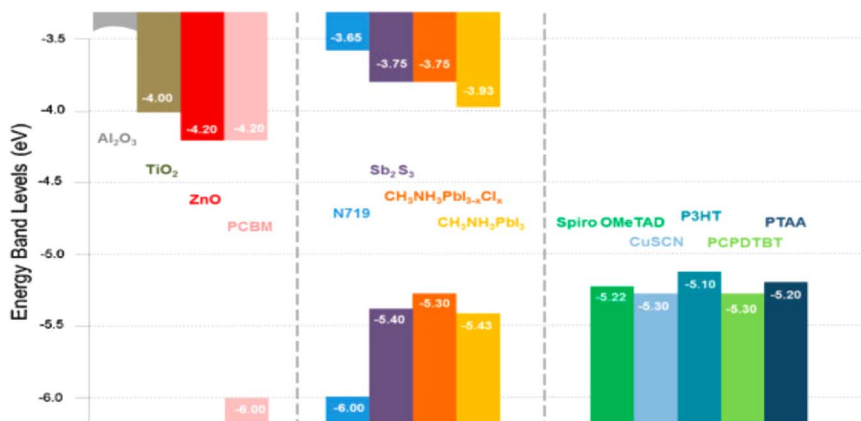
Fig. 10. Energy levels for different materials acting as a hole transporting materials (right), absorbers (middle) and an electron transporting material (left) in solar cells [75].
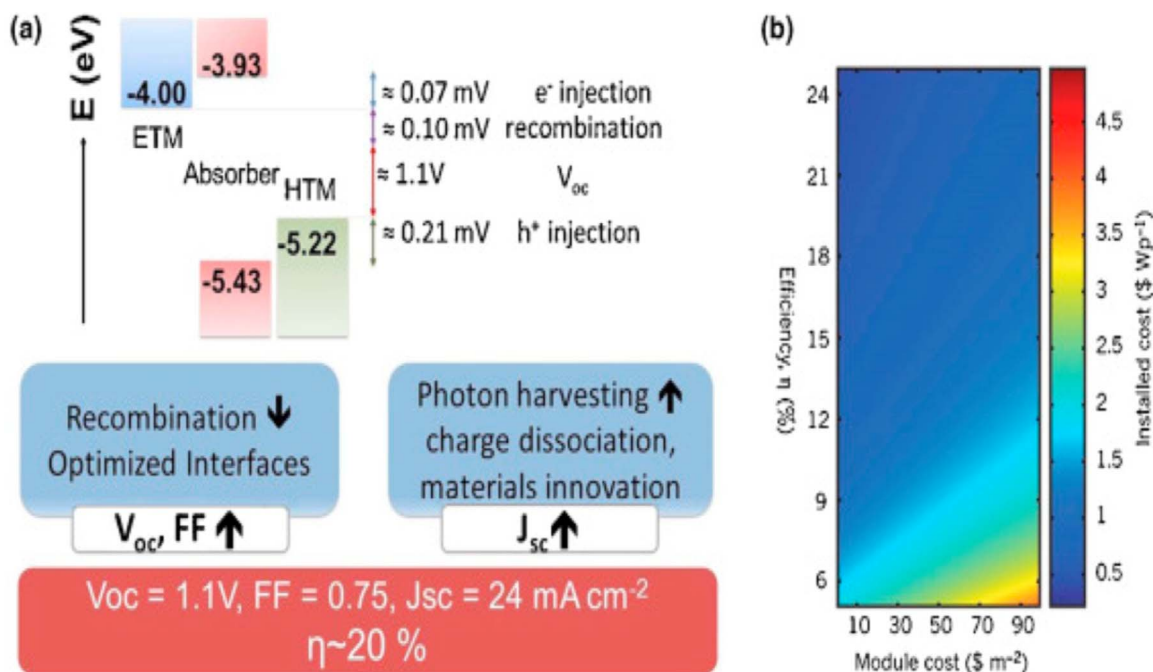
Fig. 11. a) Energetics losses and possible avenues for performance improvements in perovskites-based solar cells and (b) cost per Watt peak (Wp) as a function of efficiency and module cost [82].

by morphological deformation, metal diffusion, movable additives and so forth. Kwon et al. [91] utilized HTMs like spiroOMeTAD, poly-3-hexyl thiophene (P$_3$HT) and PDPPDBTE ((pol y[2,5-bis (2-octyldodecyl) pyrro-lo [3,4-c] pyrrole-1,4 (2 H,5 H)-dione-(E)−1,2-di (2,2'-bithiophen-5-yl) ethene]) in PSC. They found that spiroMeOTAD-based devices illuminated a reduction around 28% in PCE when ageing was extended. This value is lower when compared to the initial PCE value. PDPPDBTE-based cells improved the stability remarkably even after 1000 h. This is mainly because of its hydrophobic reaction which precluded water flow inside the perovskite. Recently, copper oxide and nickel oxide inorganic HTM-based PSC have reached an efficiency of approximately 17%, this is close to the value of organic HTM-based PSC. Moreover, the stability of inorganic HTMs is relatively better than spiroOMeTAD. Kamat and coworkers used copper iodide (CuI) as HTM in PSC and obtained a PCE of ~6.0% [92]. Interestingly, they observed improved open circuit voltage (VOC) when comparing with the greatest spiroOMeTAD devices. Impedance spectroscopy showed that CuI exhibited two orders of magnitude greater electrical conductivity compare to the spiroOMeTAD that allowed appreciably higher fill factor (FF). Recently, CuSCN has been used as HTM in PSC and considerably high PCE has been achieved [93,94]. Ito et al.[93], reported that planar TiO$_2$/CH$_3$NH$_3$PbI$_3$/CuSCN solar cells with JSC of 14.5 mA cm^2, open circuit voltage of 0.63 and FF of 0.53, yielded PCE of 4.9%. Qin et al. [94] reported PCE of 12.4% with CuSCN as an HTM using well-established sequential deposition method. Sarkar and co-workers developed inverse glass/FTO/NiO/CH$_3$NH$_3$PbI$_{3−x}$Cl$_x$/PCBM solar cells and achieved PCE of 7.3% [95]. In 2014, Yin et al.[96] used NiOx-based PSC on an ITO-glass substrate helped achieve optimal PCE of 16.47% by spin coating a presynthesized high-quality NiOx nanoparticle solution [96].

Several researchers also recently found that Lanthanum (La)–doped BaSnO$_3$ (LBSO) perovskite would be an ideal replacement given its electron mobility and electronic structure but LBSO cannot be synthesized that well whereby it dispersed fine particles or became crystallized below 500 ºC. We report a superoxide colloidal solution route for preparing an LBSO electrode under very mild conditions (below 300 ºC). The LBSO-based PSCs could retain 93% of its initial performance after 1000 h, whereas the TiO$_2$ cell completely degraded within 500 h. The development of the n-type BSO perovskite moves us

a step closer to PSC commercialization by eliminating the requirement of the additional UV filter for pervious TiO$_2$ PSCs [34].

However, all concerns have not been well addressed [97]. For commercialization of a PSC solar device, stability is a major issue. Although few researches highlight controlling the device stabilities relating to moisture, temperature, light and oxygen, other concerns like intrinsic stabilities at the interface and device architecture remain as major obstructions to practical applications. Notably, these latest results show the significant improvement in PCE and stability of PSCs by considering the possibility of using one or two optional layers together with three different mixed-halide perovskites and a few diverse of HTMs. Other significant aspects in PSCs include the ease of fabrication and similar design strategy of dye-sensitized and organic solar cells which in turn result an increase in research works in this category rapidly. During the last five years, the number of articles published on PSC devices has rapidly increased to thousands. Therefore, PSC has a significant impact in the commercialization of future generation of photovoltaic. Table 3 summarizes the growth of PSC since 2009 with a change in its material composition and improvement in efficiency.

9. Conclusion

A brief discussion based on the perovskite solar cells related to organolead halides is presented in this paper. Both Organic and inorganic hybrid halide perovskite solar cells are viable and are comparable with other photovoltaic methods because of their exclusive benefits such as Near-perfect crystallinity at low temperature and low-cost, easy fabrication and earth abundance. It is concluded that the minor "loss-in-potential" value in a solar cell leads the VOC of the greatest perovskite cells that can be higher than 1.1 V. This value almost higher than the conventional DSSCs organic solar cells that are 0.7−0.8 eV and also CdTe which is 0.59 eV. Therefore, it always can be a potential competitor for the crystal silicon solar cells (1.1 eV).

Also it is illustrated that the large charge carrier diffusion length 1 μm for mixed-halide perovskite (CH$_3$NH$_3$PbI$_{3−x}$Cl$_x$) thin films is much greater than the other thin films processed in low-temperature solution.

Table 3
summary of the efficiencies obtained from various perovskite solar cells.

Year	Perovskite	HTM	Efficiency (%)	Reference
2009	$CH_3NH_3PbI_3$	I^-/I^{-3}	3.8	[44]
2011	$CH_3NH_3PbI_3$	I^-/I^{-3}	6.5	[43]
2012	$CH_3NH_3PbI_3$	Spiro-OMeTAD	9.7	[23]
2012	$CH_3NH_3PbI_{3-x}Cl_x$	Spiro-OMeTAD	10.9	[22]
2013	$CH_3NH_3PbI_3$	PTAA	12.0	[24]
2013	$CH_3NH_3PbI_{3-x}Br_x$	PTAA	12.3	[25]
2013	$CH_3NH_3PbI_3$	Spiro-OMeTAD	15.0	[74]
2013	$CH_3NH_3PbI_3$	Spiro-OMeTAD	15.2	[51]
2014	$CH_3NH_3PbI_{3-x}Br_x$	PTAA	16.2	[31]
2014	$CH_3NH_3PbI_{3-x}Cl_x$	Spiro-OMeTAD	19.3	[32]
2014	$CH_3NH_3PbI_3$	CuI	6.0	[92]
2014	$CH_3NH_3PbI_3$	CuSCN	4.9	[93]
2014	$CH_3NH_3PbI_3$	CuSCN	12.4	[94]
2014	$CH_3NH_3PbI_{3-x}Cl_x$	NiO	7.3	[95]
2015	$CH(NH_2)^2PbI_3$	Spiro-OMeTAD	20.1	[33]
2016	$CH_3NH_3PbI_3$	NiOx	16.47	[96
2017	$CH_3NH_3PbI_3$	LBSO	21.2	34]

Therefore, the application in thin film optoelectronics has been exploited with considerable progress intensively. The high-efficiency perovskite solar cells are obtained by using LBSO and methylammonium lead iodide (MAPbI$_3$) demonstrate a steady-state power conversion of 21.2% efficiency. The LBSO-based PSCs could retain 93% of its initial performance after 1000 h of full sun illumination.

The higher potentials for the perovskite solar cell respect to the excellent optoelectronic characteristic of organometal halide perovskite material which is more desirable than high-efficiency GaAs. As the high VOC announced from organometal halide perovskite is related to higher internal photoluminescence efficiency of quantum, proper monitoring of the luminescent characteristic of perovskite can later improve the VOC, thus, resulting in higher PCE. The environmental and photostabilities should be defined when the device is used commercially. To achieve this, encapsulation materials and method with humidity-resistance and photo-stability should be established. One of the major tasks for having environmental friendly perovskite solar cells is to find other elements to replace Pb. The perovskite technology leads the high quantity production of solar cells that are high efficient and work in low temperature, which results a significant cost reduction in manufacturing procedure.

Acknowledgement

References

[1] Green MA, et al. Solar cell efficiency tables (version 40). Prog Photovolt: Res Appl 2012;20(5):606–14.

[2] Green MA. Silicon solar cells: evolution, high-efficiency design and efficiency enhancements. Semicond Sci Technol 1993;8(1):1.

[3] Britt J, Ferekides C. Thin-film CdS/CdTe solar cell with 15.8% efficiency. Appl Phys Lett 1993;62(22):2851–2.

[4] Repins I, et al. 19·9%-efficient ZnO/CdS/CuInGaSe2 solar cell with 81·2% fill factor. Prog Photovolt: Res Appl 2008;16(3):235–9.

[5] Graetzel M, et al. Materials interface engineering for solution-processed photo-voltaics. Nature 2012;488(7411):304–12.

[6] Halls JJM, et al. Efficient photodiodes from interpenetrating polymer networks. Nature 1995;376(6540):498–500.

[7] O'Regan B, Gratzel M. A low-cost, high-efficiency solar cell based on dye-sensitized colloidal TiO$_2$ films. Nature 1991;353(6346):737–40.

[8] Tang CW. Two-layer organic photovoltaic cell. Appl Phys Lett 1986;48(2):183–5.

[9] Todorov TK, Reuter KB, Mitzi DB. High-efficiency solar cell with earth-abundant liquid-processed absorber. Adv Mater 2010;22(20):E156–E159.

[10] Li G, et al. High-efficiency solution processable polymer photovoltaic cells by self-organization of polymer blends. Nat Mater 2005;4(11):864–8.

[11] Green MA, Ho-Baillie A, Snaith HJ. The emergence of perovskite solar cells. Nat Photon 2014;8(7):506–14.

[12] Hodes G, Cahen D. Photovoltaics: perovskite cells roll forward. Nat Photon 2014;8(2):87–8.

[13] Heo JH, et al. Hysteresis-less inverted CH$_3$NH$_3$PbI$_3$ planar perovskite hybrid solar cells with 18.1% power conversion efficiency. Energy Environ Sci 2015;8(5):1602–8.

[14] Heo JH, et al. Planar CH$_3$NH$_3$PbI$_3$ perovskite solar cells with constant 17.2% average power conversion efficiency irrespective of the scan rate. Adv Mater 2015;27(22):3424–30.

[15] Snaith HJ. Perovskites: the emergence of a new era for low-cost, high-efficiency solar cells. J Phys Chem Lett 2013;4(21):3623–30.

[16] Park N-G. Perovskite solar cells: an emerging photovoltaic technology. Mater Today 2015;18(2):65–72.

[17] Gratzel M. The light and shade of perovskite solar cells. Nat Mater 2014;13(9):838–42.

[18] Research cell efficiency records. NREL 2015.

[19] Burschka J, et al. Sequential deposition as a route to high-performance perovskite-sensitized solar cells. Nature 2013;499(7458):316–9.

[20] Liu M, Johnston MB, Snaith HJ. Efficient planar heterojunction perovskite solar cells by vapour deposition. Nature 2013, [Advance online publication].

[21] Zhang W, et al. Highly efficient perovskite solar cells with tunable structural color. Nano Lett 2015;15(3):1698–702.

[22] Lee MM, et al. Efficient hybrid solar cells based on meso-superstructured organometal halide perovskites. Science 2012;338(6107):643–7.

[23] Kim H-S, et al. Lead iodide perovskite sensitized all-solid-state submicron thin film mesoscopic solar cell with efficiency exceeding 9%. Sci Rep 2012;2:591.

[24] Heo JH, et al. Efficient inorganic-organic hybrid heterojunction solar cells containing perovskite compound and polymeric hole conductors. Nat Photonics 2013;7(6):486–91.

[25] Noh JH, et al. Chemical management for colorful, efficient, and stable inorganic–organic hybrid nanostructured solar cells. Nano Lett 2013;13(4):1764–9.

[26] Zhang W, et al. Ultrasmooth organic–inorganic perovskite thin-film formation and crystallization for efficient planar heterojunction solar cells. Nat Commun 2015:6.

[27] Chang Y, Park C, Matsuishi K. First-principles study of the Structural and the electronic properties of the lead-Halide-based inorganic-organic perovskites (CH~3NH~3) PbX~ 3 and CsPbX~ 3 (X= Cl, Br, I). J Korean Phys Soc 2004;44:889–93.

[28] Frost JM, et al. Atomistic origins of high-performance in hybrid halide perovskite solar cells. Nano Lett 2014;14(5):2584–90.

[29] Brivio F, Walker AB, Walsh A. Structural and electronic properties of hybrid perovskites for high-efficiency thin-film photovoltaics from first-principles. APL Mater 2013;1(4):042111.

[30] Umari P, Mosconi E, De Angelis F. Relativistic GW calculations on CH$_3$NH$_3$PbI$_3$ and CH$_3$NH$_3$SnI$_3$ perovskites for solar cell applications. Sci Rep 2014;4:4467.

[31] Jeon NJ, et al. Solvent engineering for high-performance inorganic–organic hybrid perovskite solar cells. Nat Mater 2014;13(9):897–903.

[32] Zhou H, et al. Interface engineering of highly efficient perovskite solar cells. Science 2014;345(6196):542–6.

[33] Yang WS, et al. High-performance photovoltaic perovskite layers fabricated through intramolecular exchange. Science 2015;348(6240):1234–7.

[34] Shin SS, et al. Colloidally prepared La-doped BaSnO$_3$ electrodes for efficient, photostable perovskite solar cells. Science 2017;356(6334):167–71.

[35] Baikie T, et al. Synthesis and crystal chemistry of the hybrid perovskite (CH$_3$NH$_3$) PbI$_3$ for solid-state sensitised solar cell applications. J Mater Chem A 2013;1(18):5628–41.

[36] Sum TC, Mathews N. Advancements in perovskite solar cells: photophysics behind the photovoltaics. Energy Environ Sci 2014;7(8):2518–34.

[37] Lin Q, et al. Electro-optics of perovskite solar cells. Nat Photon 2015;9(2):106–12.

[38] D'Innocenzo V, et al. Excitons versus free charges in organo-lead tri-halide perovskites. Nat Commun 2014:5.

[39] Ponseca CS, et al. Organometal halide perovskite solar cell materials rationalized: ultrafast charge generation, high and microsecond-long balanced mobilities, and slow recombination. J Am Chem Soc 2014;136(14):5189–92.

[40] Dong QF, et al. Electron-hole diffusion lengths > 175 mu m in solution-grown CH$_3$NH$_3$PbI$_3$ single crystals. Science 2015;347(6225):967–70.

[41] Xing G, et al. Long-range balanced electron- and hole-transport lengths in organic-inorganic CH$_3$NH$_3$PbI$_3$. Science 2013;342(6156):344–7.

[42] Stranks SD, et al. Electron-hole diffusion lengths exceeding 1 μm in an organometal trihalide perovskite absorber. Science 2013;342(6156):341–4.

[43] Im J-H, et al. 6.5% efficient perovskite quantum-dot-sensitized solar cell. Nanoscale 2011;3(10):4088–93.

[44] Kojima A, et al. Organometal halide perovskites as visible-light sensitizers for photovoltaic cells. J Am Chem Soc 2009;131(17):6050–1.

[45] Mosconi E, et al. First-principles modeling of mixed halide organometal perovskites for photovoltaic applications. J Phys Chem C 2013;117(27):13902–13.

[46] Koutselas IB, Ducasse L, Papavassiliou GC. Electronic properties of three- and low-dimensional semiconducting materials with Pb halide and Sn halide units. J Phys: Condens Matter 1996;8(9):1217.

[47] Zhang M, et al. Composition-dependent photoluminescence intensity and pro-longed recombination lifetime of perovskite CH$_3$NH$_3$PbBr$_3$-xCl$_x$ films. Chem Commun 2014;50(79):11727–30.

[48] Cai B, et al. High performance hybrid solar cells sensitized by organolead halide perovskites. Energy Environ Sci 2013;6(5):1480–5.

[49] Giorgi G, et al. Small photocarrier effective masses featuring ambipolar transport in

methylammonium lead iodide perovskite: a density functional analysis. J Phys Chem Lett 2013;4(24):4213–6.

[50] Ogomi Y, et al. CH₃NH₃SnₓPb₍₁₋ₓ₎I₃ Perovskite solar cells covering up to 1060 nm. J Phys Chem Lett 2014;5(6):1004–11.

[51] Liu M, Johnston MB, Snaith HJ. Efficient planar heterojunction perovskite solar cells by vapour deposition. Nature 2013;501(7467):395–8.

[52] Kim H-S, et al. Lead iodide perovskite sensitized all-solid-state submicron thin film mesoscopic solar cell with efficiency exceeding 9%. Sci Rep 2012;2:591.

[53] Etgar L, et al. Mesoscopic CH₃NH₃PbI₃/TiO₂ heterojunction solar cells. J Am Chem Soc 2012;134(42):17396–9.

[54] Jeng J-Y, et al. CH₃NH₃PbI₃ perovskite/fullerene planar-heterojunction hybrid solar cells. Adv Mater 2013;25(27):3727–32.

[55] Weber D. CH₃NH₃PbX₃, ein Pb(II)-system mit kubischer perowskitstruktur/ CH₃NH₃PbX₃, a Pb(II)-system with cubic perovskite structure. Z für Nat B 1978:1443.

[56] Kim H-S, et al. High efficiency solid-state sensitized solar cell-based on submicrometer rutile TiO₂ nanorod and CH₃NH₃PbI₃ perovskite sensitizer. Nano Lett 2013;13(6):2412–7.

[57] Arend H, et al. Layer perovskites of the (CₙH₂ₙ+1NH₃)2MX₄ and NH₃(CH₂) mNH₃MX₄ families with M= Cd, Cu, Fe, MnORPd and X= ClORBr: importance, solubilities and simple growth techniques. J Cryst Growth 1978;43(2):213–23.

[58] Umebayashi T, et al. Electronic structures of lead iodide based low-dimensional crystals. Phys Rev B 2003;67(15):155405.

[59] Baikie T, et al. Synthesis and crystal chemistry of the hybrid perovskite (CH₃NH₃) PbI₃ for solid-state sensitised solar cell applications. J Mater Chem A 2013;1(18):5628–41.

[60] Mitzi DB. Synthesis, structure, and properties of organic-inorganic perovskites and related materials. Prog Inorg Chem 2007;48:1–121.

[61] Mitzi DB, Chondroudis K, Kagan CR. Design, structure, and optical properties of organic– inorganic perovskites containing an oligothiophene chromophore. Inorg Chem 1999;38(26):6246–56.

[62] Zhang S, et al. Synthesis and optical properties of novel organic–inorganic hybrid nanolayer structure semiconductors. Acta Mater 2009;57(11):3301–9.

[63] Tanaka K, et al. Comparative study on the excitons in lead-halide-based perovskite-type crystals CH₃NH₃PbBr₃CH₃NH₃PbI₃. Solid State Commun 2003;127(9):619–23.

[64] Papavassiliou GC, Mousdis GA, Koutselas I. Some new organic–inorganic hybrid semiconductors based on metal halide units: structural, optical and related properties. Adv Mater Opt Electron 1999;9(6):265–71.

[65] Mosconi E, et al. First-principles modeling of mixed halide organometal perovskites for photovoltaic applications. J Phys Chem C 2013;117(27):13902–13.

[66] Bi D, et al. Using a two-step deposition technique to prepare perovskite (CH₃NH₃PbI₃) for thin film solar cells based on ZrO₂ and TiO₂ mesostructures. RSC Adv 2013;3(41):18762–6.

[67] Jeng JY, et al. Nickel oxide electrode interlayer in CH₃NH₃PbI₃ perovskite/PCBM planar-heterojunction hybrid solar cells. Adv Mater 2014;26(24):4107–13.

[68] Eperon GE, et al. Morphological control for high performance, solution-processed planar heterojunction perovskite solar cells. Adv Funct Mater 2014;24(1):151–7.

[69] Chen Q, et al. Planar heterojunction perovskite solar cells via vapor-assisted solution process. J Am Chem Soc 2014;136(2):622–5.

[70] Zhao Y, Zhu K. Solution chemistry engineering toward high-efficiency perovskite solar cells. J Phys Chem Lett 2014;5(23):4175–86.

[71] Liang PW, et al. Additive enhanced crystallization of solution-processed perovskite for highly efficient planar-heterojunction solar cells. Adv Mater 2014;26(22):3748–54.

[72] Zuo C, Ding L. An 80.11% FF record achieved for perovskite solar cells by using the NH4Cl additive. Nanoscale 2014;6(17):9935–8.

[73] Xiao Z, et al. Thin-film semiconductor perspective of organometal trihalide perovskite materials for high-efficiency solar cells. Mater Sci Eng: R: Rep 2016;101:1–38.

[74] Burschka J, et al. Sequential deposition as a route to high-performance perovskite-sensitized solar cells. Nature 2013;499(7458):316–9.

[75] Boix PP, et al. Current progress and future perspectives for organic/inorganic perovskite solar cells. Mater Today 2014;17(1):16–23.

[76] Heo JH, et al. Sb2S3-sensitized photoelectrochemical cells: open circuit voltage enhancement through the introduction of poly-3-hexylthiophene interlayer. J Phys Chem C 2012;116(39):20717–21.

[77] Nayak PK, et al. Photovoltaic efficiency limits and material disorder. Energy Environ Sci 2012;5(3):6022–39.

[78] Bi D, et al. Using a two-step deposition technique to prepare perovskite (CH₃NH₃PbI₃) for thin film solar cells based on ZrO₂ and TiO₂ mesostructures. Rsc Adv 2013;3(41):18762–6.

[79] Edri E, et al. High open-circuit voltage solar cells based on organic–inorganic lead bromide perovskite. J Phys Chem Lett 2013;4(6):897–902.

[80] Etgar L, et al. Mesoscopic CH₃NH₃PbI₃/TiO₂ heterojunction solar cells. J Am Chem Soc 2012;134(42):17396–9.

[81] Snaith HJ. Estimating the maximum attainable efficiency in dye-sensitized solar cells. Adv Funct Mater 2010;20(1):13–9.

[82] Graetzel M, et al. Materials interface engineering for solution-processed photovoltaics. Nature 2012;488(7411):304–12.

[83] Boix PP, et al. Hole transport and recombination in all-solid Sb₂S₃-sensitized TiO₂ solar cells using CuSCN as hole transporter. J Phys Chem C 2011;116(1):1579–87.

[84] Boschloo G, Hagfeldt A. Photoinduced absorption spectroscopy of dye-sensitized nanostructured TiO₂. Chem Phys Lett 2003;370(3):381–6.

[85] Shen Q, et al. Optical absorption, photoelectrochemical, and ultrafast carrier dynamic investigations of TiO₂ electrodes composed of nanotubes and nanowires sensitized with CdSe quantum dots. Jpn J Appl Phys 2006;45(6S):5569.

[86] Bisquert J, et al. Electron lifetime in dye-sensitized solar cells: theory and interpretation of measurements. J Phys Chem C 2009;113(40):17278–90.

[87] Wang M, et al. An organic redox electrolyte to rival triiodide/iodide in dye-sensitized solar cells. Nat Chem 2010;2(5):385–9.

[88] Bi D, et al. Effect of different hole transport materials on recombination in CH₃NH₃PbI₃ perovskite-sensitized mesoscopic solar cells. J Phys Chem Lett 2013;4(9):1532–6.

[89] Ball JM, et al. Low-temperature processed meso-superstructured to thin-film perovskite solar cells. Energy Environ Sci 2013;6(6):1739–43.

[90] Xing G, et al. Long-range balanced electron-and hole-transport lengths in organic-inorganic CH₃NH₃PbI₃. Science 2013;342(6156):344–7.

[91] Kwon YS, et al. A diketopyrrolopyrrole-containing hole transporting conjugated polymer for use in efficient stable organic–inorganic hybrid solar cells based on a perovskite. Energy Environ Sci 2014;7(4):1454–60.

[92] Christians JA, Fung RC, Kamat PV. An inorganic hole conductor for organo-lead halide perovskite solar cells. Improved hole conductivity with copper iodide. J Am Chem Soc 2013;136(2):758–64.

[93] Ito S, et al. Carbon-double-bond-free printed solar cells from TiO₂/CH₃NH₃PbI₃/ CuSCN/Au: structural control and photoaging effects. ChemPhysChem 2014;15(6):1194–200.

[94] Qin P, et al. Inorganic hole conductor-based lead halide perovskite solar cells with 12.4% conversion efficiency. Nat Commun 2014:5.

[95] Subbiah AS, et al. Inorganic hole conducting layers for perovskite-based solar cells. J Phys Chem Lett 2014;5(10):1748–53.

[96] Yin X, et al. Highly efficient flexible perovskite solar cells using solution-derived NiOₓ hole contacts. ACS Nano 2016;10(3):3630–6.

[97] Berhe TA, et al. Organometal halide perovskite solar cells: degradation and stability. Energy Environ Sci 2016;9(2):323–56.